

A Fabrication Process and Analysis of ZnO-ZnS-Sb₂S₃ Thin Film Solar Cells

by
David Spencer Catherall

A THESIS

submitted to
Oregon State University
Honors College

in partial fulfillment of
the requirements for the
degree of

Honors Baccalaureate of Science in Chemical Engineering
(Honors Scholar)

Presented May 19, 2020
Commencement June 2020

AN ABSTRACT OF THE THESIS OF

David Spencer Catherall for the degree of Honors Baccalaureate of Science in Chemical Engineering presented on May 19, 2020. Title: A Fabrication Process and Analysis of ZnO-ZnS-Sb₂S₃ Thin Film Solar Cells.

Abstract approved: _____

Chih-hung Chang

The purpose of this research is to provide a simple fabrication method for zinc oxide and antimony sulfide based thin film solar cells. Both a ZnO nanorod electron conducting structure and a stibnite absorber show promise in a solar cell. Initial attempts at using only ZnO and Sb₂S₃, however, resulted in destruction of the ZnO. An intermediary ZnS layer was included to mitigate this issue. Cells were created by chemical bath deposition (CBD) of ZnO nanorods, chemical treatment to partially convert the ZnO to ZnS, CBD deposition of amorphous Sb₂S₃, and crystallization by annealing under N₂. The films were analyzed by SEM, EDX, UV-Vis, and dark current-voltage response. SEM shows ZnO nanorods 340 nm thick, a thin Zn(O,S) layer, and 240 nm Sb₂S₃ layer. UV-Vis shows near-absolute absorption at 300-400 nm, with absorptivity decreasing from 99.9% to 90% across wavelengths of 400-800 nm. Tauc plots show band gaps of 3.2, 3.6, and 1.6 eV for ZnO, ZnS, and Sb₂S₃, respectively, which correspond to literature. Dark IV analysis shows a thin film diode response. Future work will entail improvements in film uniformity, process repeatability, and additional SEM analysis. Further research is also proposed to measure device efficiency, needing only the further deposition of P3HT, PEDOT:PSS, and a conductive metallic layer.

Key Words: Sb₂S₃, antimony sulfide, ZnO, nanorods, thin film, solar cell, photovoltaics

Corresponding e-mail address: David.S.Catherall@gmail.com

©Copyright by David Spencer Catherall
May 19, 2020

A Fabrication Process and Analysis of ZnO-ZnS-Sb₂S₃ Thin Film Solar Cells

by
David Spencer Catherall

A THESIS

submitted to
Oregon State University
Honors College

in partial fulfillment of
the requirements for the
degree of

Honors Baccalaureate of Science in Chemical Engineering
(Honors Scholar)

Presented May 19, 2020
Commencement June 2020

Honors Baccalaureate of Science in Chemical Engineering project of David Spencer Catherall presented on May 19, 2020.

APPROVED:

Chih-hung Chang, Mentor, representing Chemical, Biological, and Environmental Engineering

Zhongwei Gao, Committee Member, representing Chemical, Biological, and Environmental Engineering

Nick AuYeung, Committee Member, representing Chemical, Biological, and Environmental Engineering

Toni Doolen, Dean, Oregon State University Honors College

I understand that my project will become part of the permanent collection of Oregon State University, Honors College. My signature below authorizes release of my project to any reader upon request.

David Spencer Catherall, Author

Acknowledgements

I would like to thank Dr. Chih-hung Chang for supporting myself and the research for this thesis, especially by providing access to necessary lab space and materials. I also give much thanks to Dr. Zhongwei Gao for aiding the project from its inception, in providing guidance from procedures to research direction, and performing or overseeing characterization of samples.

Table of Contents

1. Introduction	1
2. Background	2
2.1 Photovoltaics as a Green Energy Solution	2
2.2 Photovoltaic Mechanisms	2
2.3 Current Technology.....	3
2.4 Sb ₂ S ₃ -Based Solar Cells	3
2.5 ZnS Band Offset Issue.....	5
2.6 Deposition Reactions.....	6
2.7 Basis for Investigation.....	7
3. Materials and Methods	8
3.1 Materials.....	8
3.2 Methods.....	8
4. Results and Discussion	10
4.1 SEM/EDX Characterization of ZnO/Sb ₂ S ₃	10
4.2 SEM Characterization of ZnO/ZnS/Sb ₂ S ₃	11
4.3 Visual MINTEQ Simulation	13
4.4 UV-Vis Absorption Results	14
4.5 Band Gap Estimation via Tauc Plots.....	15
4.6 IV Response Curve.....	16
4.7 Future Work	17
5. Conclusion	18
Appendix	19
Bibliography	21

Table of Figures

Figure 1. Fabricated Device Schematic	4
Figure 2. Device Energy Band Diagram	5
Figure 3. ZnO/Sb ₂ S ₃ SEM	10
Figure 4. ZnO/Sb ₂ S ₃ EDX	11
Figure 5. ZnO/ZnS/Sb ₂ S ₃ SEM.....	12
Figure 6. Visual MINTEQ Results	13
Figure 7. ZnO/ZnS/Sb ₂ S ₃ UV-Vis	14
Figure 8. Figure 8. Sb _s S ₃ Annealing Effect (Visual)	15
Figure 9. Tauc Plots	16
Figure 10. Dark IV Curve	17
Figure 11. ZnO/ZnS/Sb ₂ S ₃ SEM (large).....	19
Figure 12. ZnO and ZnO/ZnS UV-Vis	19
Figure 13. Sb ₂ S ₃ Annealing Effect (SEM).....	20

1. Introduction

With the ever more pressing need to transition the world's energy sources from fossil fuels to renewables, photovoltaic (PV) technologies have become increasingly desirable. The current market-leading technology is based off doped silicon, and while reasonably efficient these panels are costly to produce, and the units are bulky. In seeking improvements in some combination of efficiency, cost, flexibility, and properties like radiation hardness, other technologies have been invented over the years. These include dye-sensitized solar cells, thin film solar cells, and other novel technologies utilizing materials such as semiconductor nanowires. Each has unique advantages over the silicon cells of today, but except for CdTe thin film solar cells, few have made their way to market.

Among emerging PV technologies, thin film solar cells are attractive for multiple reasons. They offer a wide range of manufacturing techniques, including chemical bath deposition, which makes synthesis possible with minimal specialized equipment. It is also possible to incorporate nanostructured films. Additionally, thin film solar cells also utilize only a small amount of material, since their final thicknesses can be within (or less than) the micron range (granted, some fabrication processes may result in a significant amount of waste). Sb_2S_3 is a good candidate as a material in these cells due to its nearly ideal band gap and low precursor toxicity relative to other established materials like CdS/CdTe. To create cells of entirely low toxicity materials, ZnO also has potential for use as an electron conductor. A range of hole-conductive materials may be used to complete the cell, including pre-synthesized polymers. The focus of this study was originally to create ZnO/ Sb_2S_3 cells and investigate the effects of doping on efficiency, however research facility closure required the project to end early. Therefore, the purpose of this thesis is to outline a fabrication method for future works, and to characterize the resulting device.

2. Background

2.1 Photovoltaics as a Green Energy Solution

As world energy demands increase with its ever-growing population and reliance on technology, energy production must rise to meet it. However, as of 2014 over 66.7% of the world's electricity supply was sourced from non-renewable, greenhouse-gas emitting sources.¹ It is critical to both reduce the amount of pollution generated from powering the electric grid, and to ensure the sustainability of electric power, that renewable energy sources are used. One such source is solar energy.

2.2 Photovoltaic Mechanisms

Solar cells primarily operate by taking advantage of the electronic effects that occur between two semiconducting materials that have shifted energy bands in their electronic structure. The electronic bands of a solid material determine the energy states that electrons within the material can occupy. In atoms these states, or energy levels, are very discrete. However, in solids they become virtually continuous ranges called energy bands. In photovoltaics, the important bands are the conduction and valence bands. These represent the highest occupied and lowest unoccupied energy states of electrons in the material.

In semiconductors, these states are separated by a band gap—a region of energy states electrons cannot occupy. What differentiates semiconductors from both insulators and conductors is the band gap energy, which is greater than zero but less than 3-5 eV (varies depending on source). If energy is supplied, electrons can be excited from the valence to conduction band and can return by emitting or transferring energy in some form. In solar cells this excitation energy comes from photons. Only certain photons can accomplish this, however, as they must have energy greater than the band gap. Their energy is a function of wavelength:

$$E = \frac{hc}{\lambda}$$

Where h is Planck's constant, c is the speed of light, and λ is the wavelength. The smaller the gap, the less energy is needed, and more wavelengths are useable. However, too much extra energy results in heating and inefficiency. Therefore, the ideal band gap for a solar cell using the incident solar spectrum is 1.2-1.4 eV. This is a middle ground between energy efficiency and thermal management.^{2,3}

Without a photovoltaic device structure, excited electrons simply find their way to their original state over time. However, if one of two adjacent materials has shifted bands, such that the conduction and valence band edges are higher in energy than those of the other material, electrons and electron holes experience opposing directional driving forces and an electric current is generated. Positive (P) and negative (N) type materials also selectively conduct holes and electrons, respectively, adding another cause for unlike charges to move in opposite directions. Additional effects occur when P and N-type materials are in direct contact, but this is not relevant in this project.²

2.3 Current Technology

Today's solar cells are primarily made of silicon.⁴ P and N-type material layers are created by doping, which creates the necessary electronic driving force. However, this technology has many limitations. The silicon must be manufactured with extremely high purity, which is energy intensive.⁵ The manufacturing process itself is also energy intensive due to the high temperatures needed for dopant diffusion. Many additional materials are needed in the cells, also increasing costs. While these cells generally boast efficiencies on par with or better than many emerging single junction solar cell technologies,⁶ their cost, weight, and fragility is still a major limitation in their adoption.⁷

To counter these pitfalls, other solar technology is currently under investigation. One such field of research is thin film cells. Commercial cells of this type tend to use CdTe and CdS. Recently, these cells have even started to match conventional Si-based solar cells in terms of efficiency.⁸ However, the reliance on cadmium is a large drawback due to its toxicity, so there are other thin film materials being researched.

2.4 Sb₂S₃-Based Solar Cells

The cells investigated in this project focus on a kind of cell without direct contact between P and N type materials, known as a semiconductor-sensitized solar cell. They take after dye-sensitized solar cells, which work by using an intermediary dye material for light absorption and electron excitation. In dye-sensitized cells, an electrolyte is used to conduct holes away from the absorber. In the case of semiconductor sensitized solar cells, the entire cell is solid-state.

Thus, in these devices, cells simply consist of the traditional P and N-type semiconducting layers with an absorber between them.²

The focus of this research is on Sb_2S_3 . This chalcogenide is a promising material as a solar absorber material due to its band gap of about 1.7 eV, relative abundance of elemental constituents, low melting/crystallization temperature, and relative non-toxicity when compared to other thin film PV materials (which include elements like cadmium or lead).⁹ Additionally, it is possible to deposit the material via chemical bath deposition (CBD). This method is attractive as it is low-tech and low-cost, requiring (at the lab scale) only a stir plate, small sealable container, stir bar, refrigeration unit, and a water bath. Other thin film deposition methods such as chemical vapor deposition, atomic layer deposition, and spray deposition all require expensive specialized equipment.

To be complete, a solar cell must also have hole and electron conductors on either side of the film. Typically, TiO_2 is used as the electron conducting material in related studies due to its n-type properties. However, to allow for easier deposition using less hazardous chemicals, ZnO was chosen instead as it is also n-type.¹⁰ Additionally, ZnO can be deposited in a nanorod form which improves contact area with the Sb_2S_3 . The hole conductor can be a variety of materials deposited at the end of the process, such as P3HT. The structure of the cell fabricated in this study is shown in Figure 1, while the energy band diagram of a fully developed cell is shown in Figure 2.

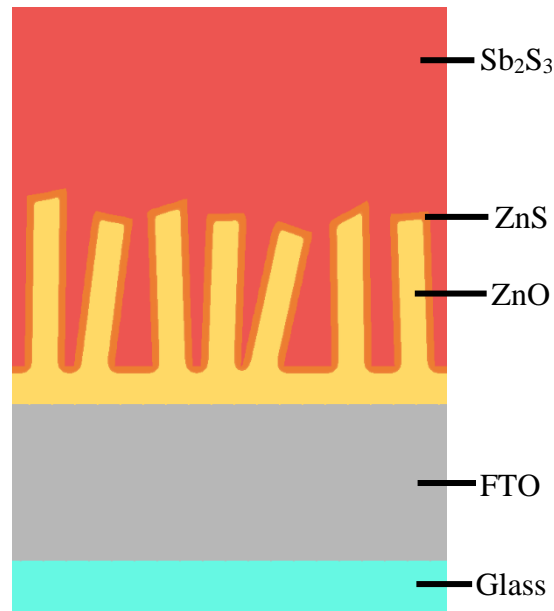


Figure 1. Fabricated device schematic, with FTO glass, ZnO nanorod structure, ZnS layer, and Sb_2S_3 absorber layer.

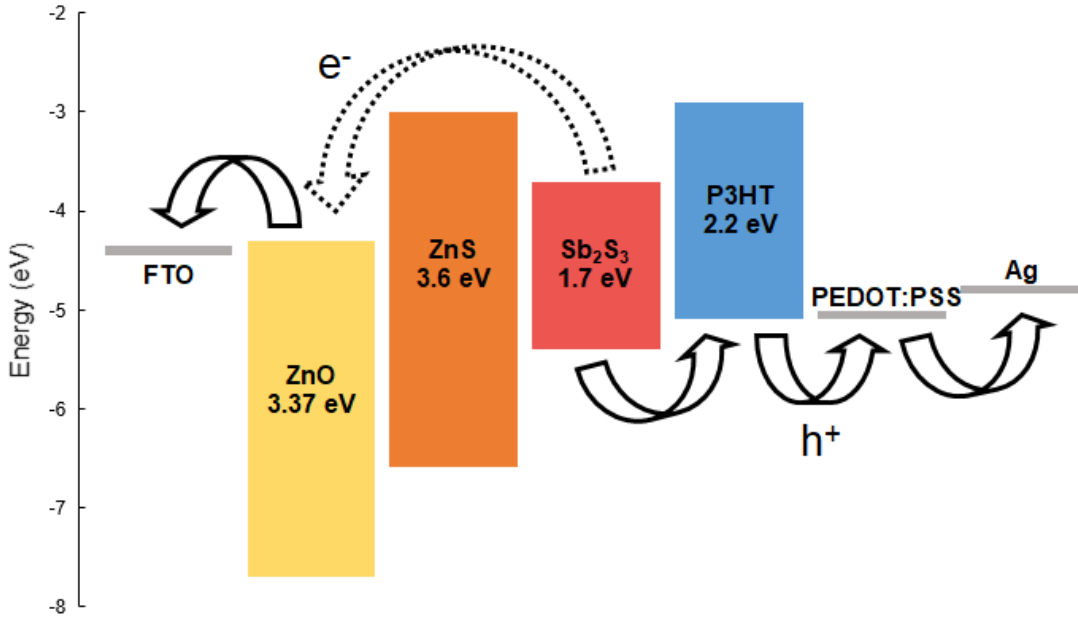


Figure 2. Energy band diagram of the proposed final photovoltaic structure. Note the energy barrier caused by ZnS—however others’ work has shown this does not prevent electron flow to the more preferential conduction band of ZnO,^{11,12} though it may decrease efficiency. Data used from Nikolakopoulou, et. al., and Parize, et. al.^{13,14}

Research into Sb_2S_3 absorber solar cells has so far yielded a maximum efficiency of 7.5%, with a theoretical efficiency of 29%. If it is used as a top subcell with traditional Si cells, such a device could even reach 40% overall efficiency.⁹ However charge recombination (excited electrons and holes recombining) has been shown to be a large factor degrading the efficiency of Sb_2S_3 solar cells.¹⁵ In mitigating this, it has been demonstrated that decreasing defects at material interfaces as well as in the absorber itself is possible via doping and surface modification.⁹ However, the discrepancy between the theoretical 29% efficiency and realized 7.5% is likely still due to unmitigated charge recombination. It is also possible the efficiency could be raised by up to 10% from existing devices by adding an antireflective layer.⁹

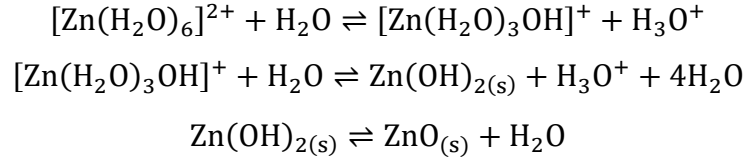
2.5 ZnS Band Offset Issue

An item of concern with the usage of a ZnS layer on the ZnO is the energy barrier it would present. As shown in Figure 2, it would take energy for the excited electrons to transfer from Sb_2S_3 to ZnS to ZnO and out of the system. Should such a system be fabricated exactly as shown, no photovoltaic effect should be observed.¹² However, it has been shown that the use of a ZnS layer created by converting ZnO does not completely block the photocurrent.^{11,12} This is likely due to the formation of $\text{Zn}(\text{O},\text{S})$ rather than pure ZnS. $\text{Zn}(\text{O},\text{S})$ has a tunable band offset,

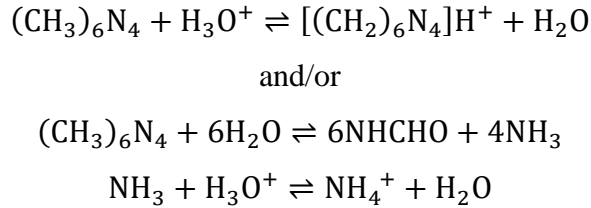
dependent on the ratio of elements.¹² Therefore, it is possible to create a ZnS-containing buffer layer while also retaining a photocurrent, so long as no pure ZnS phase is present.

2.6 Deposition Reactions

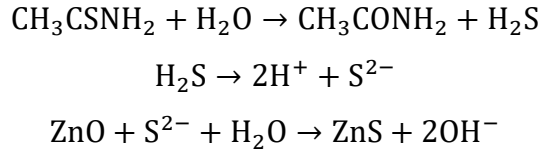
The work in this thesis is a combination of multiple device construction methods. The first method¹¹ starts with creating ZnO nanorods by the reactions:¹⁶



Where H_3O^+ is consumed by:



Then, the outer layer of ZnO is converted to ZnS by the following reactions:¹¹



In the original study this method was used in, ZnS is also partially converted to Sb_2S_3 by treatment with SbCl_3 in ethanol. The resulting thickness of Sb_2S_3 was on the order of tens of angstroms. Because the absorber material is meant to be the workhorse of the device in terms of light absorption, this thickness is not ideal. However, there exists a common method to deposit Sb_2S_3 by CBD, which can create layer thicknesses in the hundreds of nanometers—enough to absorb almost the entirety of incident light at certain wavelengths. This second method uses the reaction:¹⁷



2.7 Basis for Investigation

The combination of these methods is theoretically ideal due to the antireflective properties of ZnO nanorods,¹⁸ high contact area between layers, and strong light absorption due to a thick Sb₂S₃ layer. Constructing the films around an anti-reflective material should decrease light losses. Since Sb₂S₃ is a poor conductor, decreasing the length electrons must traverse to reach their conductor by having an imbedded nanorod structure is likely to increase efficiency. ZnO and ZnS are also easy to deposit and contain less toxic precursors than materials such as TiO₂.

It was originally within the scope of this project to investigate efficiency of a working cell and the effects of doping the Sb₂S₃, but due to facility closure the research phase of this project was cut short. Therefore, this project will investigate the synthesis of a device using ZnO nanorods and CBD deposited Sb₂S₃. Various parameters of the resulting cell will also be determined including morphology, absorptivity, and IV characteristics. The goal is to develop a low-tech fabrication process, which could prove useful in future experiments focusing on its completion and material/process optimization.

3. Materials and Methods

3.1 Materials

Chemicals used were zinc acetate dihydrate from J.T. Baker (100.9%), hexamethylenetetramine (HMTA) from Alfa Aesar (99+%), antimony chloride ($\geq 99.0\%$) and thioacetamide (99%) from Sigma-Aldrich, zinc nitrate hexahydrate, and sodium thiosulfate pentahydrate. Silicon wafers, glass, and FTO-coated glass were used as substrates for materials deposition.

3.2 Methods

Silicon, glass, and FTO-coated glass substrates were prepared by cleaning with tap water and detergent, acetone, methanol, and deionized water. This was followed by treatment in an aqueous 1 M sodium hydroxide solution. This treatment was done for 30 minutes with sonication for glass substrates, and 20 minutes without sonication for silicon and FTO-coated glass substrates.

To deposit ZnO nanorod films, a seed layer was created by spin coating with 0.02 M zinc acetate in ethanol at 1500 rpm for 40 seconds. This was followed by annealing in atmosphere at 250 °C for 1 hour. ZnO nanorods were then grown by chemical bath deposition. Substrates were suspended vertically in an equimolar solution of 0.025 M HMTA and zinc nitrate. The solution was placed in a water bath at 70 °C for 2 hours, with moderate stirring. Deposition was followed by rinsing with DI water and drying with nitrogen.

ZnS conversion was performed by following an already developed method.¹¹ ZnO-coated substrates were immersed vertically in an aqueous 0.1 M thioacetamide solution for 2.5 hours at 90 °C. No stirring was done for this step. Afterwards, substrates were washed with DI water and dried with nitrogen.

Sb₂S₃ deposition was also done following an established method.¹⁹ Solutions of 650 mg SbCl₃ in 2.5 mL acetone, and 25 mL of 1 M sodium thiosulfate were prepared. The solutions were chilled and mixed, and chilled DI water was added to make 100 mL. This was followed by vigorous stirring and suspension of the substrates at a downwards angle. The reaction was cooled to 10 °C using a water bath and stirred lightly. The reaction proceeded for 1 hour before samples were removed, rinsed with DI water, and dried with nitrogen. Annealing of Sb₂S₃ films was done

in a tube furnace under nitrogen atmosphere for 1 hour at 300 °C. The samples were also allowed to remain in the furnace until it had cooled to room temperature.

Film morphologies were observed by using SEM, while EDX was simultaneously used to analyze their compositions. Simulation of the chemical species in the Sb_2S_3 chemical bath was performed with Visual MINTEQ v3.1. UV-Vis spectroscopy was performed in the range of 200-800 nm to observe the absorbance spectrum of samples, as well as to estimate material band gaps via Tauc plots. Dark IV-curve analysis was done via the two-probe method. Electrodes were placed directly on the FTO film and on carbon paste applied to the top film.

4. Results and Discussion

4.1 SEM/EDX Characterization of ZnO/Sb₂S₃

Initial attempts at creating a ZnO and Sb₂S₃ cell by CBD deposition without a ZnS intermediary layer resulted in the structures shown in Figure 3, with EDX results shown in Figure 4. It is observed that the nanorod structure remains intact after Sb₂S₃ deposition, albeit with poor film adherence to the surface. The EDX results show, however, almost complete destruction of the ZnO nanorods as evidenced by the lack of zinc. This was confirmed with an additional sample. This conclusion is also supported by the poor adhesion of the Sb₂S₃ film to the substrate, which could be caused by the dissolution of the underlying ZnO layer, as samples with only Sb₂S₃ on FTO did not show the same problem.

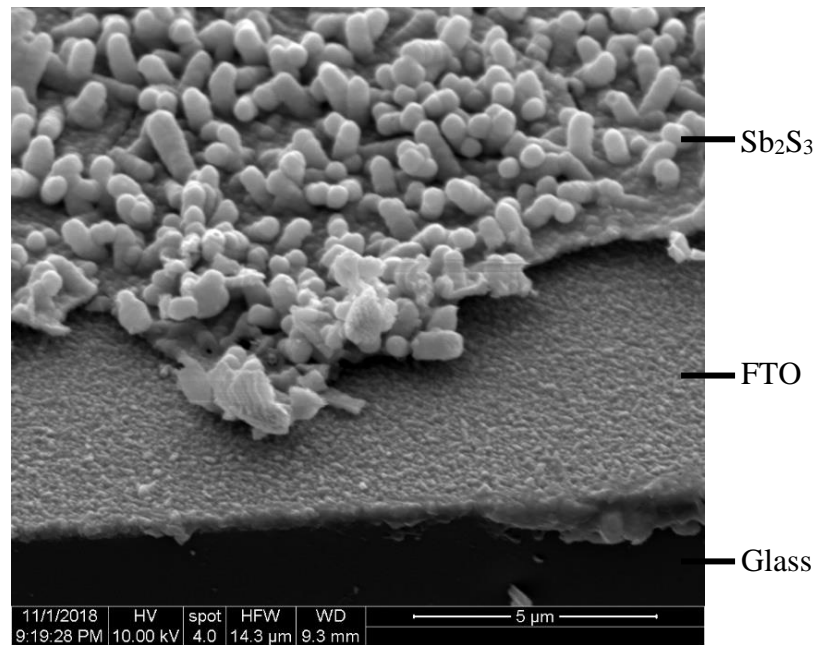


Figure 3. SEM cross-section of the structure resulting from ZnO and Sb₂S₃ deposition, on FTO-glass. The FTO layer is evident as the bottom layer across the whole substrate, while the other film/rods comprise the deposited materials. The nanorod structure formed by ZnO¹¹ is evident, however the material itself is not present.

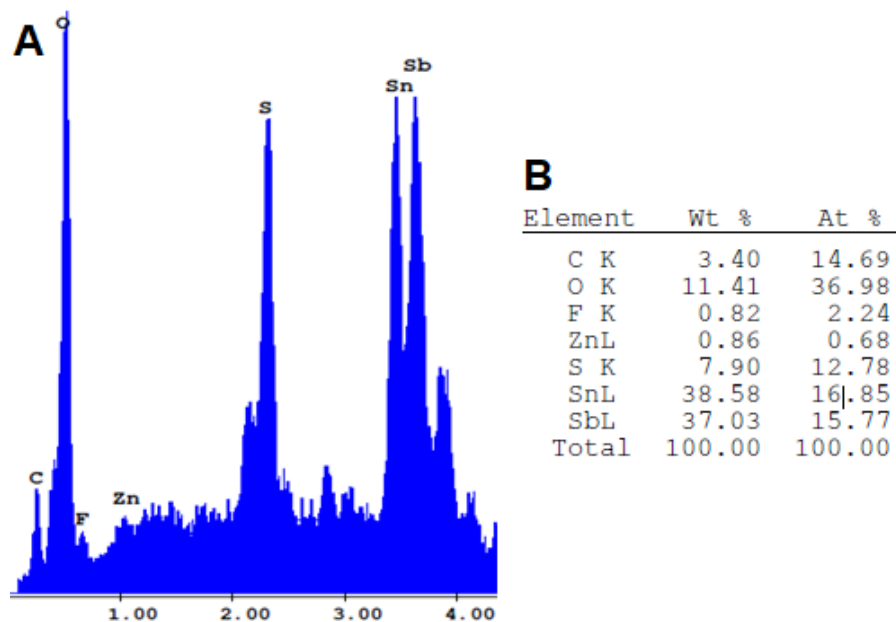


Figure 4. EDX results of the structures shown in Figure 3. **A.** Plot of EDX results, with relevant peaks (Zn, O, Sb, S, Sn, F, and C) shown. **B.** Data analysis of EDX results. The film is observed to contain less than 1 at% Zn, although with no clear peak in the data this may be attributable to noise.

It is possible that the ZnO destruction was caused by a few different factors. First, ZnO is very soluble in acidic solutions. It is possible that at some point the solution for Sb₂S₃ deposition is acidic enough to gradually dissolve the nanorods. Similarly, it is also possible that ZnO is dissolving by forming complexes with other chemicals in solution. In these scenarios, it is possible the rods dissolved slowly enough for Sb₂S₃ to deposit and maintain the shape, or dissolution started after some time. Another possibility is that the Sb₂S₃ itself may chemically attack the ZnO, forming Sb₂O₃ and leaving the zinc to form more soluble compounds. This theory is supported by the Sb:S ratio from EDX showing more antimony than sulfur, which should not be the case if the deposited material was solely Sb₂S₃. Therefore, the presence of Sb₂O₃ is likely. Regardless, due to the destruction of the ZnO observed, it was decided to include ZnS as an intermediary material.

4.2 SEM Characterization of ZnO/ZnS/Sb₂S₃

Figure 5 shows SEM results from a sample of ZnO/ZnS/Sb₂S₃ on silicon. While the existence of ZnO was not confirmed with EDX, it is plain to see the crystalline pillar structure of ZnO nanorods, distinct from the amorphous Sb₂S₃. Therefore, it is observed that the intermediary

ZnS protects the ZnO during Sb_2S_3 deposition. However, the ZnO film appears denser than the previous one used in the sample for Figure 3. In fact, while most deposited ZnO nanorod films appear clear or hazy, this sample displayed prominent thin film interference. It is likely this was the result of a thick film, rather than a field of nanorods. It is possible the lower surface area to volume ratio may have had something to do with protecting the ZnO. Regardless, further samples created did not initially display an interference pattern, but still retained the ZnO/ZnS film as confirmed through UV-Vis. These samples eventually displayed interference after ZnS conversion, which may indicate film thickening during this step, meaning the ZnO film was not very dense beforehand (SEM was not performed to confirm this).

Concerning the Sb_2S_3 film, it consists of multiple parts: a dense bottom layer, and a disperse field of nanoparticles both in and on top of the dense layer. It is likely these two morphologies formed from direct growth on the ZnS surface, and from deposition of particles grown in solution, respectively. The existence of the former growth method is supported by the presence of a very smooth film with no visible boundaries from particle growth. The existence of the latter growth method is supported both by the visible presence of Sb_2S_3 precipitation in the bath solution, as well as the fact that some particles have centers far outside the dense film and could not have grown from it.

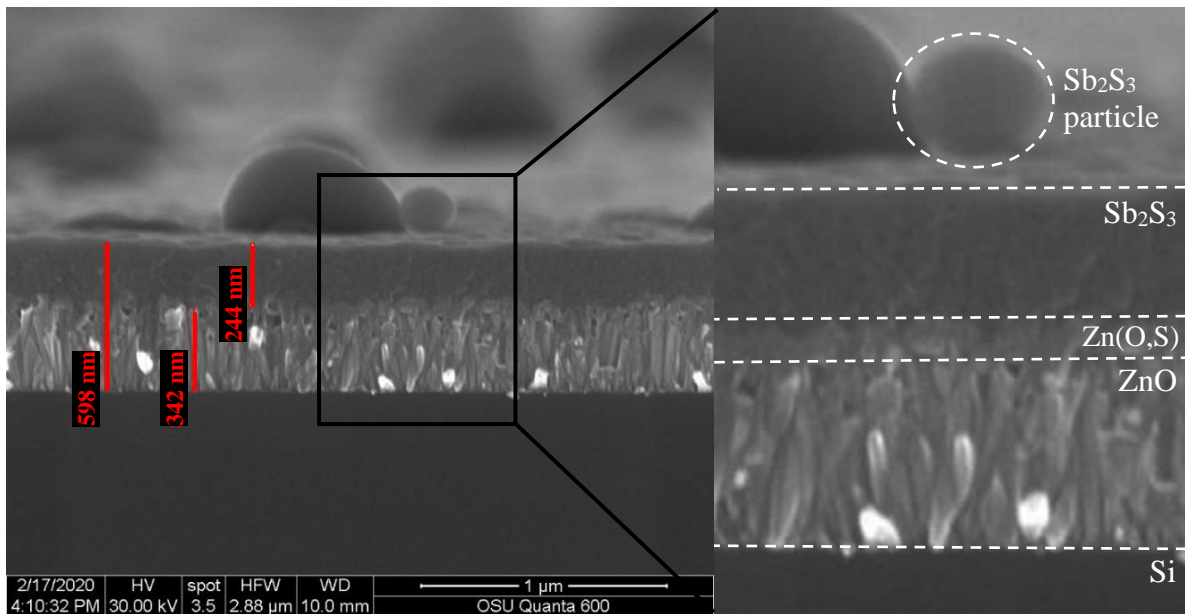


Figure 5. SEM cross-section of the unannealed ZnO/ZnS/ Sb_2S_3 structure on a silicon substrate. ZnO appears as a thick nanorod structure (bottom) approximately 340 nm thick, Zn(O,S) (middle) 20 nm thick, and Sb_2S_3 (top) 240 nm thick. It is also observed that there are Sb_2S_3 particles across the surface. See Figure 11 for a less magnified image.

4.3 Visual MINTEQ Simulation

To provide insight into theories regarding the dissolution of ZnO and protection by ZnS, the equilibrium chemical species in the Sb_2S_3 deposition process were calculated with Visual MINTEQ. Results from simulating the zinc species equilibria are shown in Figure 6. The range of possible pH values for the reaction solution are also shown, and the exact value varies depending on mixing order and reaction progress. The minimum pH corresponds to a chemical bath with only SbCl_3 , while the maximum corresponds to the complete solution at equilibrium. The thermodynamic equilibrium and species solubilities lead to the prediction that ZnO will be unstable at all possible pH values and will dissolve, primarily complexed by thiosulfate ions. Meanwhile, ZnS is stable. While the simulation is not entirely complete due to the lack of $\text{Sb}_2(\text{S}_2\text{O}_3)_3$ and the inability to simulate possible reactions between Sb_2S_3 and ZnO, neither issue should have a dramatic impact on the chemistry leading to the dissolution of ZnO. Therefore, these predictions lend support to the theory that the solution used is harmful to ZnO because of the formation of soluble complexes.

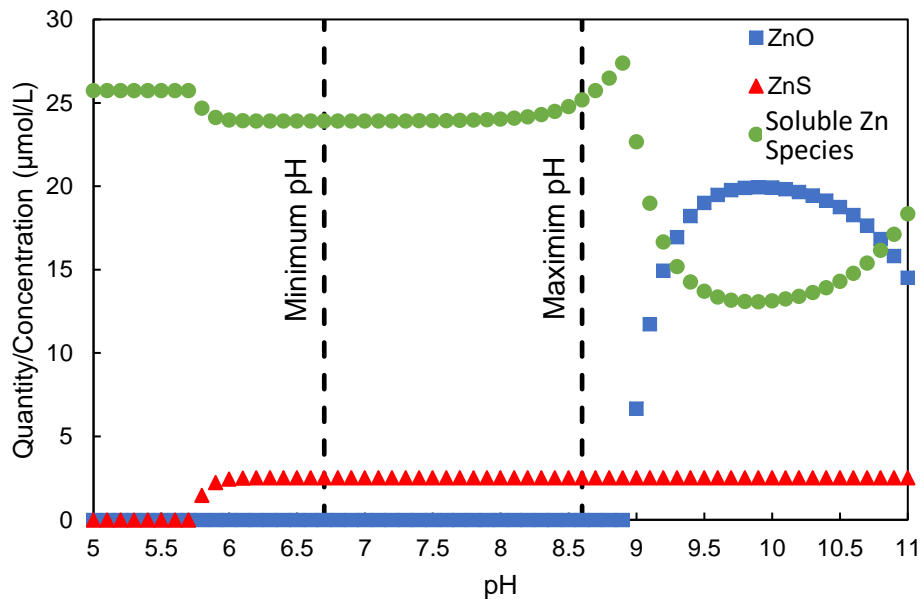


Figure 6. Visual MINTEQ results for the Sb_2S_3 deposition bath, with zinc species shown. ZnO shown as squares, ZnS as triangles, and soluble species as circles. Minimum pH and maximum pH represent the range of possibilities depending on mixing order and reaction progress. It is observed that ZnO is unstable (no amount present) at all possible reaction pH values, while ZnS is stable (nonzero quantity). Above pH 9, ZnO starts to become a stable species, but this pH is not expected to occur.

4.4 UV-Vis Absorption Results

Figure 7 shows the absorption spectrum of the film stack at different process steps. The absorption spectrum of ZnO and Sb_2S_3 are clear,^{20,21} with the peak corresponding to ZnS (just under 300 nm)²² not apparent, possibly indicating the amount is very small (however, there is a spectral change after ZnO to ZnS conversion, supporting the presence of ZnS, as shown in Figure 12). The results show an increase in absorption across the entire spectrum as Sb_2S_3 is deposited on ZnO/ZnS, and again after it is annealed. The dramatic change caused by annealing the Sb_2S_3 film is caused by the change in crystal structure. Deposited Sb_2S_3 forms an orange-yellow colored amorphous film and annealing the film results in a metallic-brown/black color shown in Figure 8A. As expected, the darker, more intense color corresponds to increased absorption. The visual transitions between other process steps are also shown in Figure 8B. Of additional note is that wavelengths between 300 and 400 nm in the final structure are absorbed almost completely, while the absorbance tapers down from 3 to 1 (99.9% to 90%) over the visible spectrum. This represents a very good absorbance of light, critical for PV performance.

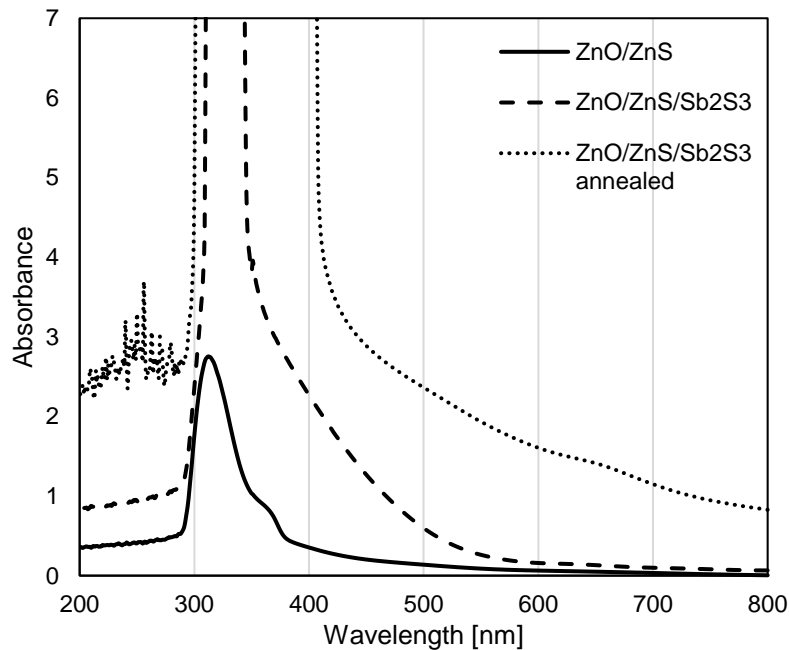


Figure 7. UV-Vis spectral absorbance results for ZnO/ZnS/ Sb_2S_3 film on FTO-glass. ZnO/ZnS, ZnO/ZnS/ Sb_2S_3 unannealed, and ZnO/ZnS/ Sb_2S_3 annealed shown as solid, dashed, and dotted lines, respectively. It is observed that the peak around 315 nm grows and expands towards longer wavelengths with each successive process step. The final film stack is observed to absorb from 90% to over 99.99% of light between 300-800 nm, depending on the wavelength.

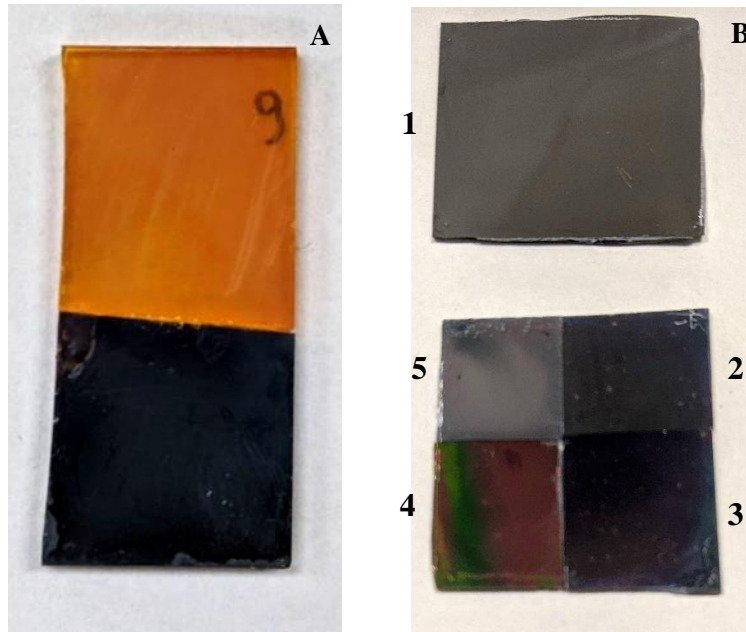


Figure 8. A. Comparison of unannealed (top) and annealed (bottom) Sb_2S_3 film. Film is solely Sb_2S_3 , deposited with a 3 hour deposition time on glass. Annealed at 300 °C for 30 minutes in nitrogen. SEM images of similar unannealed/annealed samples shown in Figure 13. **B.** Comparison of samples (on silicon) at various process points. 1. Bare silicon 2. ZnO 3. ZnO/ZnS 4. ZnO/ZnS/ Sb_2S_3 (unannealed) 5. ZnO/ZnS/ Sb_2S_3 (annealed). Although not entirely clear in the image, thin film interference starts with sample 3, and becomes more pronounced with sample 4.

4.5 Band Gap Estimation via Tauc Plots

The Tauc plot interpretation of the UV-Vis data for the annealed ZnO/ZnS/ Sb_2S_3 sample from Figure 7 is shown in Figure 9. It is observed that each film has a distinct band gap, at 3.2 eV, 3.6 eV, and 1.6 eV corresponding to ZnO, ZnS, and Sb_2S_3 respectively. These values are approximately what is expected. ZnO is often reported to have a gap between 3.1 and 3.37 eV,²³ ZnS is reported to have a gap of 3.6 eV,¹⁴ and while the gap of Sb_2S_3 is often reported as between 1.7 and 2.5 eV,⁹ 1.6 eV is within the values found by some groups.²⁴ Besides confirming the near-ideal band gap for Sb_2S_3 , the match between the literature and observed values for all materials lends support to their presence (direct measurements by EDX or other methods was not done on these samples). With a band gap of 1.6 eV, the fabricated Sb_2S_3 film should be able to utilize the entire visible spectrum, which is critical since this material is the workhorse of the device in terms of solar energy conversion. It may also be possible to further decrease the band gap via doping, allowing additional longer wavelengths to become useful²⁵.

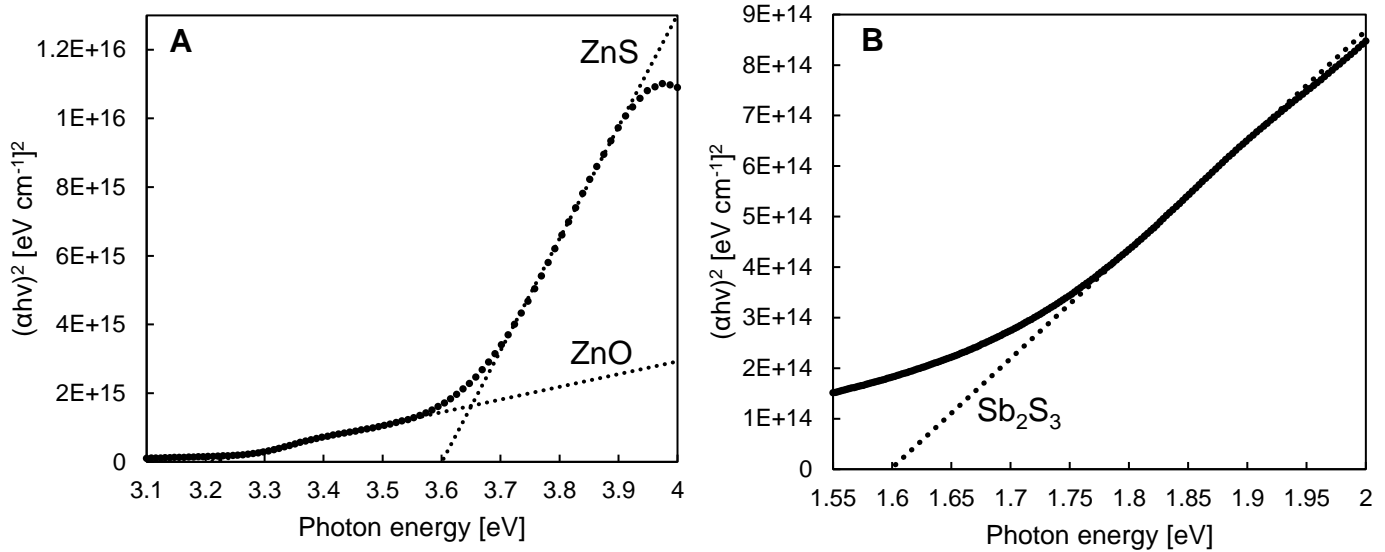


Figure 9. Tauc plots for a ZnO/ZnS/Sb₂S₃ annealed structure, with a 2.5 hour deposition time for Sb₂S₃. Substrate was FTO glass. **A.** Lines for ZnO and ZnS. Corresponding band gaps are 3.2 and 3.6 eV, respectively. **B.** Line for Sb₂S₃. Observed band gap is 1.6 eV.

4.6 IV Response Curve

Figure 10 shows the dark IV-response of the samples used for Figure 7. It is observed that any sample with at least the ZnO/ZnS interface exhibits a diode response. Further, the response decreases when Sb₂S₃ is deposited but increases slightly when the film is annealed. These results show promise in the functionality of a PV device, since it is desirable that electron flow only be allowed in one direction. However, during testing it was noted that these results varied with the position on the sample, likely corresponding to the film quality in that location. There were defects visible under optical microscope, and while care was taken to test good quality areas of the films, it is likely that defects existed that were too small to be seen visually. These small defects may be the cause of the uncharacteristically linear shape of the ZnO/ZnS line, and the noise in the other two. Future experiments will need to have additional focus on maintaining clean samples between processes, and in film uniformity during ZnO and Sb₂S₃ depositions.

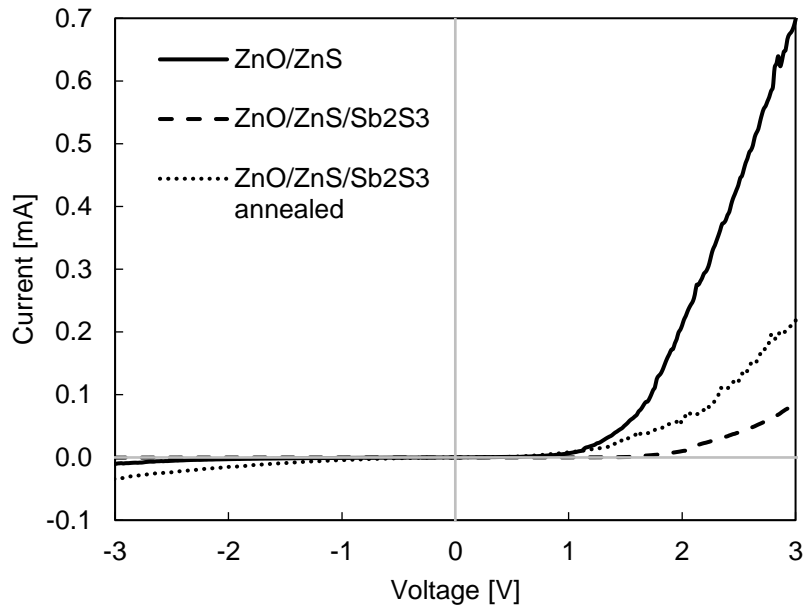


Figure 10. Dark IV-curve for ZnO/ZnS/Sb₂S₃ structures on FTO-glass. ZnO/ZnS, ZnO/ZnS/Sb₂S₃ unannealed, and ZnO/ZnS/Sb₂S₃ annealed shown as solid, dashed, and dotted lines, respectively. All film structures show thin film diode behavior, albeit with some noticeable noise in the data for the three-component films. This is possibly due to film imperfections, as defects could be seen under optical microscopy, especially in the annealed film.

4.7 Future Work

There remains much to be done to complete and further the research performed in this project. Much of the characterization presented was done on samples with poor film quality. With additional time, better samples could be made. SEM analysis of samples analogous to those used for UV-Vis and IV characterization has also yet to be done. It is also suggested that further tests to find device efficiency be conducted. For such an analysis, the addition of P3HT, PEDOT:PSS, and a thin metal layer (preferably Ag) is required. Additional future work can also be done by optimizing or changing the properties of the ZnS/Zn(O,S) and Sb₂S₃ layers. Since pure ZnS represents an energy barrier, controlling the conduction band level by modifying the ratio of the Zn(O,S) material present is necessary. There is an optimal value to be found, as there is a drop in photocurrent at both the low and high extremes of the O:S ratio.¹² Charge recombination in Sb₂S₃, theorized to be a large limiter on its performance, may also be mitigated by film modification. This and other film characteristics (such as band gap) can be enhanced via doping to increase efficiency.^{26,27}

5. Conclusion

The fabrication of a photovoltaic device utilizing ZnO nanorods and Sb₂S₃ as a semiconductor sensitizer has been demonstrated. It was found that the inclusion of an intermediary ZnS layer is necessary to protect the nanorods during the Sb₂S₃ deposition step, which can be done by simple aqueous chemical treatment of the ZnO layer. Without it, the ZnO likely dissolves due to the formation of soluble complexes. Sb₂S₃ can then be deposited by a common CBD method. The resulting structure shows thicknesses of ZnO and Sb₂S₃ in the 300-200 nm range. SEM also shows uniformity of the ZnO and ZnS layers, but the Sb₂S₃ deposition step resulted in nanoparticles in addition to a dense film. UV-Vis spectroscopy shows that after annealing, the absorption of visible wavelengths ranges from 90% to 99.9%. 300-400 nm light is almost completely absorbed. Analysis of the material band gaps via Tauc plots yields values consistent with literature of 3.2, 3.6, and 1.6 eV for ZnO, ZnS, and Sb₂S₃, respectively. The device also demonstrates a diode response under dark IV characterization. No IV curve under light nor efficiency measurements were collected due to closure of research facilities.

There remains much that can be done to both provide additional data for the experiments conducted and to build on this fabrication method. Some characterization could not be done, including SEM on samples used for UV Vis and IV curve measurements. The full device including a hole-conducting layer has not yet been fabricated and is necessary for efficiency measurements. Further studies could be performed on optimization of each layer. Namely, ZnO nanorod density and height, Zn(O,S) ratio and thickness, Sb₂S₃ thickness, and annealing conditions could be adjusted. Film modification by doping is also of interest, due to its demonstrated effects on efficiency. This project has demonstrated only the feasibility of a device using relatively abundant and nontoxic materials, and there is much available work to complete and expand this research.

Appendix

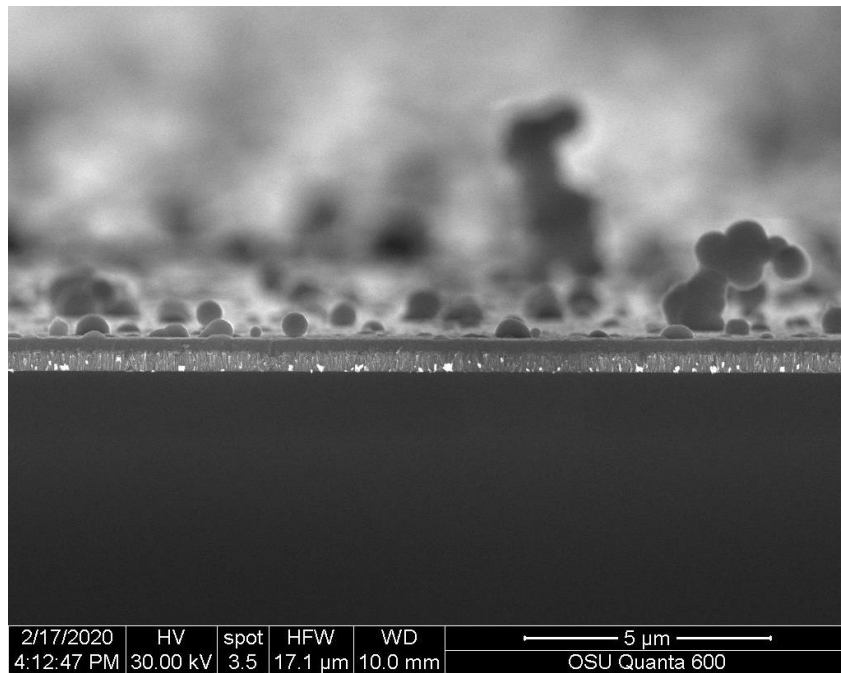


Figure 11. SEM cross-section of the unannealed ZnO/ZnS/Sb₂S₃ structure on a silicon substrate. Zoomed out image of the same sample as seen in Figure 5. Shows broader view of uniform dense films, and nanoparticles across the surface.

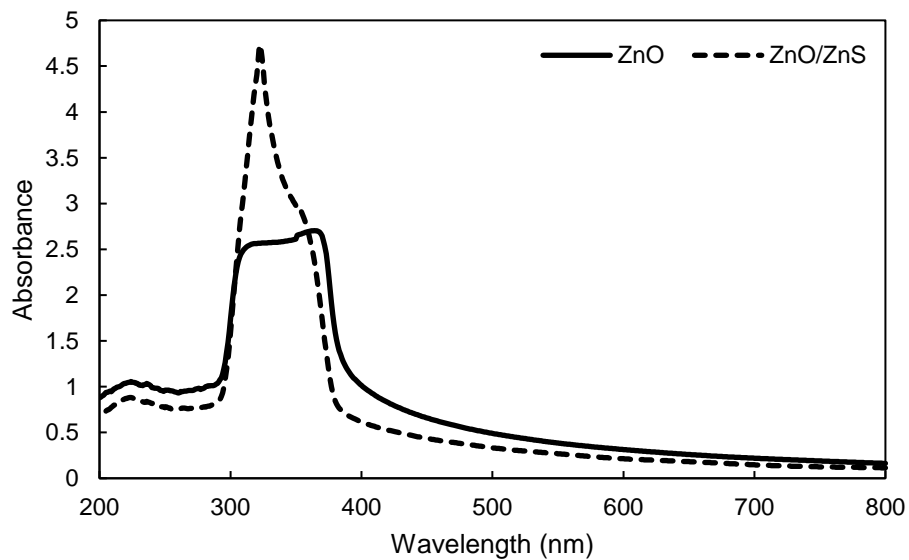


Figure 12. UV-Vis spectrum of ZnO (solid line) and ZnO/ZnS (dashed line) structures. Glass substrate used, with a 3 hour ZnO to ZnS conversion time.

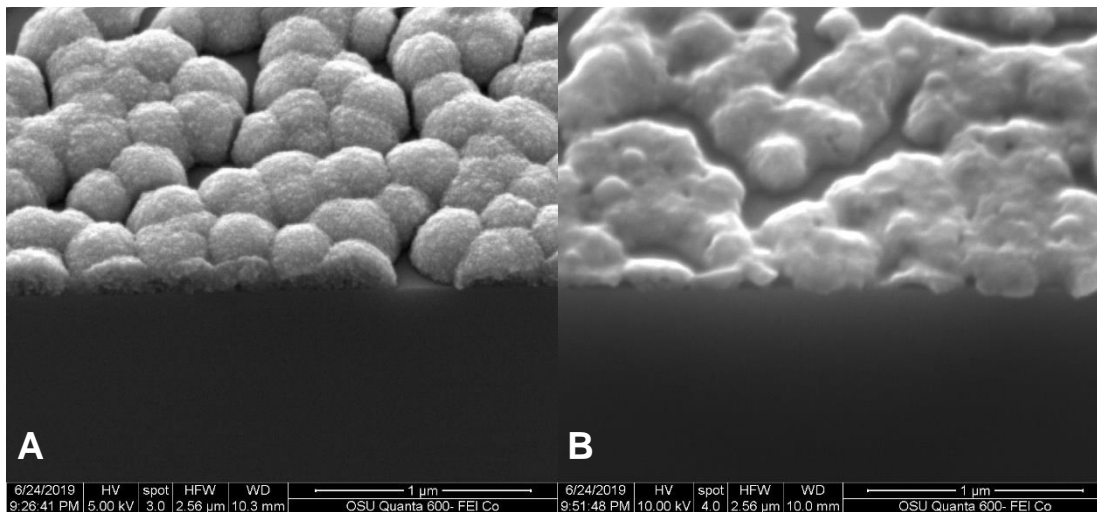


Figure 13. SEM cross-section of unannealed Sb_2S_3 (**A**) and annealed Sb_2S_3 (**B**) films. Deposited on silicon. A morphology change is evident due to the material's low phase transition temperatures.

Bibliography

- ¹ Breeze, P. *Electricity Generation and the Environment*; Elsevier Science and Technology, 2017; pp 6.
- ² Würfel, P.; Würfel, U. Basic Structure of Solar Cells. In *Physics of Solar Cells From Basic Principles to Advanced Concepts*, 3rd Ed.; Wiley-VCH: Weinheim, Germany, 2016, pp 128-133.
- ³ Rühle, S. Tabulated Values of the Shockley-Queisser Limit for Single Junction Solar Cells. *Sol. Energy*, **2016**, 130, 139-147.
- ⁴ Crystalline Silicon Photovoltaics Research. US Department of Energy Web site.
<https://www.energy.gov/eere/solar/crystalline-silicon-photovoltaics-research> (Accessed Apr 4, 2020).
- ⁵ Pizzini, S. Towards Solar Grade Silicon: Challenges and Benefits for Low Cost Photovoltaics. *Sol. Energ. Mat. Sol. C.*, **2010**, 94, 1528-1533.
- ⁶ Best Research-Cell Efficiency Chart. National Renewable Energy Laboratory Web Site.
<https://www.nrel.gov/pv/cell-efficiency.html> (Accessed Apr 4, 2020).
- ⁷ Battaglia, C.; Cuevas, A.; De Wolf, S. High-Efficiency Crystalline Silicon Solar Cells: Status and Perspectives. *Energ. Environ. Sci.*, **2016**, 5, 1552-1576.
- ⁸ Cadmium Telluride Solar Cells. National Renewable Energy Laboratory Web site.
<https://www.nrel.gov/pv/cadmium-telluride-solar-cells.html> (Accessed Apr 4, 2020).
- ⁹ Kondrotas, R.; Chen, C.; Tang, J. Sb₂S₃ Solar Cells. *Joule*, **2018**, 2, 5, 857-878.
[https://www.cell.com/joule/pdf/S2542-4351\(18\)30140-5.pdf](https://www.cell.com/joule/pdf/S2542-4351(18)30140-5.pdf)
- ¹⁰ Janotti, A.; Van de Walle, C. G. Fundamentals of Zinc Oxide as a Semiconductor. *Rep. Prog. Phys.*, **2009**, 72.

- ¹¹ Han, J.; Liu, Z.; Zheng, X.; Guo, K.; Zhang, X.; Hong, T.; Wang, B.; Liu, J. Trilaminar ZnO/ZnS/Sb₂S₃ Nanotube Arrays for Efficient Inorganic-Organic Hybrid Solar Cells. *RSC Adv.*, **2014**, 4, 23807.
- ¹² Ericson, T.; Scragg, J. J.; Hultqvist, A.; Wätjen, J. T.; Szaniawski, P.; Törndahl, T.; Platzer, B.; Björkman, C. Zn(O,S) Bugger Layers and Thickness Variations of CdS Buffer for Cu₂ZnSnS₄ Solar Cells. *IEEE J. Photovolt.*, **2014**, 4, 1, 465-469.
- ¹³ Nikolakopoulou, A.; Raptis, D.; Dracopoulos, V.; Sygellou, L.; Andrikopoulos, K. S.; Lianos, P. Study of Upscaling Possibilities for Antimony Sulfide Solid State Sensitized Solar Cells. *J. Power Sources*, **2015**, 278, 404-410.
- ¹⁴ Parize, R.; Katerski, A.; Gromyko, I.; Rapenne, L.; Roussel, H.; Kärber, E.; Appert, E.; Krunk, M.; Consonni, V. ZnO/TiO₂/Sb₂S₃ Core-Shell Nanowire Heterostructure for Extremely Thin Absorber Solar Cells. *J. Phys. Chem. C*, **2017**, 121, 18, 9672-9680.
- ¹⁵ Darga, A.; Mencaraglia, D.; Longeaud, C.; Savenije, T. J.; O'Regan, B.; Bourdais, S.; Muto, T.; Delatouche, B.; Dennier, G. On Charge Carrier Recombination in Sb₂S₃ and its Implication for the Performance of Solar Cells. *J. Phys. Chem. C*, **2013**, 117, 40, 20525-20530.
- ¹⁶ Strano, V.; Urso, R. G.; Scuderi, M.; Iwu, K. O.; Simone, F.; Ciliberto, E.; Spinella, C.; Mirabella, S. Double Role of HMTA in ZnO Nanorods Grown by Chemical Bath Deposition. *J. Phys Chem. C*, **2014**, 118, 48, 28189-28195.
- ¹⁷ Maghraoui-Meherzi, H.; Nasr, T. B.; Kamoun, N.; Dachraoui, M. Physical Properties of Chemically Deposited Sb₂S₃ Thin Films. *Cr. Chim.*, **2011**, 14, 5, 471-475.
- ¹⁸ Ko, Y. H.; Yu, J. S. Structural and Antireflective Properties of ZnO Nanorods Synthesized Using the Sputtered ZnO Seed Layer for Solar Cell Applications. *J. Nanosci. Nanotechnol.*, **2010**, 10, 8095-8101.
- ¹⁹ Rodriguez-Lazcano, Y.; Guerrero, L.; Daza, O. G.; Nair, M. T. S.; Nair, P. K. Antimony Chalcogenide Thin Films: Chemical Bath Deposition and Formation of New Materials by Post Deposition Thermal Processing. *Superficies Vacio*, **1999**, 9, 100-103.

- ²⁰ Ocakoglu, K.; Mansour, S. A.; Yildirimcan, S.; Al-Ghamdi, A. A.; El-Tantawy, F.; Yakuphanoglu, F. Microwave-Assisted Hydrothermal Synthesis and Characterization of ZnO Nanorods. *Spectrochim. Acta, Part A*, **2015**, 148, 362-368.
- ²¹ Krishnan, B.; Arato, A.; Cardenas, E.; Das Roy, T. K.; Castillo, G. A. On the Structure, Morphology, and Optical Properties of Chemical Bath Deposited Sb₂S₃ Thin Films. *Appl. Surf. Sci.*, **2008**, 254, 10, 3200-3206.
- ²² Li, Z. Q.; Shi, J. H.; Liu, Q. Q.; Wang, Z. A.; Sun, Z.; Huang, S. M. Effect of [Zn]/[S] Ratios on the Properties of Chemical Bath Deposited Zinc Sulfide Thin Films. *Appl. Surf. Sci.*, **2010**, 257, 1, 122-126.
- ²³ Srikant, V.; Clarke, D. R. On the Optical Band Gap of Zinc Oxide. *J. Appl. Phys.*, **1998**, 83, 5447.
- ²⁴ Radzwan, A.; Ahmed, R.; Shaari, A.; Lawal, A.; Ng, Y. X. First-Principles Calculation of Antimony Sulphide Sb₂S₃. *Mal. J. Fund. Appl. Sci.*, **2017**, 13, 3, 285-289.
- ²⁵ Ito, S.; Tsujimoto, K.; Nguyen, D.; Manabe, K.; Nishino, H. Doping Effects in Sb₂S₃ Absorber for Full-Inorganic Printed Solar Cells with 5.7% Conversion Efficiency. *Int. J. Hydrogen Energy*, **2013**, 38, 36, 16749-16754.
- ²⁶ Jiang, C.; Tang, R.; Wang, X.; Ju, H.; Chen, G.; Chen, T. Alkali Metals Doping for High-Performance Planar Heterojunction Sb₂S₃ Solar Cells. *Solar RRL*, **2018**, 3, 1.
- ²⁷ Tang, R.; Wang, X.; Jiang, C.; Li, S.; Liu, W.; Ju, H.; Yang, S.; Zhu, C.; Chen, T. n-Type Doping of Sb₂S₃ Light-Harvesting Films Enabling High-Efficiency Planar Heterojunction Solar Cells. *ACS Appl. Mater. Inter.*, **2018**, 10, 36, 30314-30321.

